



Effect of cathodic micro-discharges on oxide growth during plasma electrolytic oxidation (PEO)

Alexandre Nominé,, J. Martin, Gérard Henrion, Thierry Belmonte

► To cite this version:

Alexandre Nominé,, J. Martin, Gérard Henrion, Thierry Belmonte. Effect of cathodic micro-discharges on oxide growth during plasma electrolytic oxidation (PEO). Surface and Coatings Technology, 2015, 269, pp.131-137. 10.1016/j.surfcoat.2015.01.076 . hal-03612228

HAL Id: hal-03612228

<https://hal.univ-lorraine.fr/hal-03612228>

Submitted on 6 Feb 2023

HAL is a multi-disciplinary open access archive for the deposit and dissemination of scientific research documents, whether they are published or not. The documents may come from teaching and research institutions in France or abroad, or from public or private research centers.

L'archive ouverte pluridisciplinaire **HAL**, est destinée au dépôt et à la diffusion de documents scientifiques de niveau recherche, publiés ou non, émanant des établissements d'enseignement et de recherche français ou étrangers, des laboratoires publics ou privés.



Distributed under a Creative Commons Attribution - NonCommercial - NoDerivatives 4.0 International License

Effect of cathodic micro-discharges on oxide growth during Plasma Electrolytic Oxidation (PEO)

A. Nominé, J. Martin, G. Henrion, T. Belmonte

Institut Jean Lamour, UMR7198 CNRS - Université de Lorraine, – Department of chemistry and physics of solids and surfaces, Parc de Saurupt – CS 50840, F-54011 Nancy cedex France

Abstract

Plasma Electrolytic Oxidation (PEO) of magnesium alloy is performed in NH_4F and KOH based electrolytes within various waveforms of bipolar current pulses in order to investigate the role of the cathodic biasing on both the growth mechanisms of the PEO coating and the micro-discharge behaviour. A particular attention is paid to the cathodic micro-discharges and their appearance (or not) depending on the process conditions. Although cathodic micro-discharges are shown to have detrimental effect on the PEO layer, it is pointed out that cathodic biasing is necessary to improve the growth of the oxide coatings. Conditions that promote cathodic breakdown are discussed and a mechanism of cathodic breakdown of the layer is proposed. Meanwhile, it is evidenced that cathodic micro-discharges, and to a greater extent cathodic biasing, influences the anodic breakdown coming immediately after, and therefore the process behaviour during the anodic biasing.

Keywords: plasma electrolytic oxidation (PEO), magnesium, breakdown, micro-discharges, bipolar current pulse.

Highlights:

- A mechanism of cathodic breakdown of the PEO layer is proposed.
- Cathodic micro-discharges are found to be detrimental to the coating growth.
- The mutual influence of cathodic and anodic biasing is pointed out.
- Size and lifetime of cathodic micro-discharge are determined in the range 0.15-0.45 mm² and 100-150 μs respectively.

1. Introduction

Plasma electrolytic oxidation is a promising surface treatment that might replace conventional anodizing to grow thick protective oxide coatings on light alloys (*e.g.* Al, Mg, Ti...). Although, both processes consist in immersing a work electrode and one or several counter electrodes in a conductive electrolyte, the physical mechanisms of oxide growth are basically different. In anodizing, oxide growth is driven by redox reactions and follows the Faraday law. The coating thickness is limited to some tens of micrometres with growth rates of hundreds of nanometres per minute. On the other hand, due to the high current density (1-100 A.dm⁻²) and voltage (400 – 1000V) applied during the PEO process, micro-discharges (MDs for short) are repeatedly ignited at the surface of the substrate [1]. Therefore, PEO allows fast synthesis of coatings with thicknesses reaching hundreds of micrometres in a few tens of minutes [2-5]. The breakdown of oxides layers by MDs is considered as the principal mechanism that contributes to the oxide growth. The influence of the discharge features on the properties of the PEO layers has been already reported [6, 13]. For instance, Mécuson *et al* [14, 15] showed that a judicious setting of the cathodic current half-period parameters (amplitude, duration) with respect to the anodic ones induces a voltage drop associated with the quasi disappearance of MDs. This regime, called the “soft regime”, improves the compactness, growth rate and corrosion resistance of the layers. Nevertheless, though the role of the cathodic half-period was clarified, no MDs were observed under cathodic biasing. However, we recently showed that within specific conditions, cathodic MDs could be observed [16]. Surprisingly, no anodic MDs were detected, and the light emission corresponding to cathodic MDs has a pseudo periodic behaviour [16]. The following sections will show the influence of cathodic MDs on the oxide growth. The influence of one current half-period (either anodic or cathodic) on the one coming immediately after (cathodic or anodic, resp.) will be pointed out.

2. Experimental procedure

The process is carried out on commercial EV31 magnesium alloy substrates (table 1) in alcalino-silicate ($[\text{KOH}] = 0.036 \text{ mol.L}^{-1} + [\text{Na}_2\text{SiO}_3] = 0.016 \text{ mol.L}^{-1}$) and ammonium fluoride ($[\text{NH}_4\text{F}] = 0.27 \text{ mol.L}^{-1}$) electrolytes. The current is supplied by a pulsed generator (Ceratronic[®]) that can deliver several types of waveforms as shown in table 2. The light emitted by the MDs was recorded with a Hamamatsu R928 photomultiplier (PM) whose output signal was amplified by a 300 MHz bandwidth current amplifier (Stanford Research Systems SR445). The PM signal as well as current and voltage waveforms were collected and recorded using a 1 GHz bandwidth oscilloscope (Agilent 54832B). Space and time properties of MDs like their size, overall number and mean lifetime were determined from the analysis of images recorded using a Photron Fastcam SA1.1 ultra-high speed video camera (UHSC) whose acquisition rate was set at 125 kHz. Due to the important volume of data, images were processed using the TRACE software [17, 18].

Oxide layer composition and morphology were characterized with a Philips XL30 scanning emission microscope equipped with a field-emission gun (FEG) and an EDX detector. Samples were cut, mounted in resin at low temperature and low pressures in order to let the resin penetrate the oxide layer. Then, samples were polished through successive grades of SiC abrasive papers and finely polished to 1 μm with diamond paste. In order to avoid charge accumulation during SEM investigations, samples were covered with a thin layer of gold, deposited by sputtering. Phase composition was investigated by X-ray diffraction (XRD), using a INEL diffractometer equipped with a Co $K\alpha$ anticathode ($\lambda = 1.78897 \text{ \AA}$).

3. Results and discussion

3.1. Characterisation of coatings

The surface of the samples oxidized in conditions that promote the formation of cathodic MDs (current signal WAVE1, NH_4F electrolyte), exhibits an extremely rough surface visible to the naked eye. The SEM top-view micrograph shown in figure 1 shows large pores spread in a foamy layer. Flakes are visible (fig. 1a) and the oxide even peels off in places (fig. 1b).

Cross section micrographs (fig. 2) show that substrate is strongly corroded. This might greatly contribute to the roughness of the sample. They also confirm the localized delamination of the coating. Unlike usual PEO layers, the oxides formed in NH_4F electrolytes have a structure in strata (fig. 2c). Apparently the strata do not adhere either to the substrate or to each other.

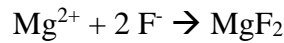
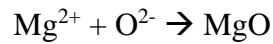
The EDX spectrum of the synthesized coating (point 1 in fig. 2a) is presented in figure 3a. It shows intense peaks of magnesium, fluorine and oxygen due to the presence of MgO and MgF_2 in the coating. This is supported by the X-Ray diffraction pattern that clearly indicates that the coating is exclusively composed of those phases (fig. 3b). A high peak of carbon is also detected. It is attributed to the insertion of epoxy resin between strata during the encapsulation process. Besides, EDX spectra made on magnesium substrate (point 2 in fig. 2a) show a carbon peak at least five times smaller than those measured on the coating (point 1 in fig. 2a).

3.2. Role of anodic and cathodic half-periods on coating growth and breakdown

The previous results establish that treatments in NH_4F electrolyte with AC current degrade the layer properties drastically. The following study aims to determine whether those defects come from the electrolyte composition or from cathodic MDs. Thus, treatments have been made under

unipolar (either cathodic or anodic) DC pulsed current (respectively WAVE2 and WAVE3). Since under AC current, MDs appear only under cathodic biasing, it is relevant to investigate MDs under unipolar cathodic regime (WAVE2). However, and surprisingly, no MDs are observed (fig. 4). Furthermore, no oxides could be measured on the sample and no evidence of corrosion could be found. This result shows that the anodic half-period plays an important role on the generation of cathodic MDs.

Under anodic DC pulsed current (WAVE3), an oxide layer grows, though no discharges are observed (fig. 5). The oxide layer exhibits also a strata structure in these conditions (fig. 5b). The layer grows during anodic biasing and without any discharge assistance. Hence, the oxide certainly grows according to the following chemical reactions:



The layer has a fine grain size or is even partly amorphous for the oxide growth does not need any heat transfer, unlike layers grown with MDs. XRD pattern shows very low diffraction peak intensities of layer components (MgO and MgF₂) as compared to the substrate (fig. 3b). Note that the sample is only corroded under anodic biasing (fig. 5a). However, without MDs, no layer spalling occurs.

3.3. Breakdown mechanism of cathodic MDs

The physical mechanisms that lead to breakdown in liquids are complex and still under study [19-21]. Nevertheless, the aforementioned results make it possible to propose a mechanism of

cathodic breakdown. The sample is immersed in electrolyte (fig. 6a) and simultaneously corroded and oxidized (fig. 6b) under anodic biasing. Oxidation leads to the formation of a dielectric layer composed of magnesium oxide and fluoride (MgO and MgF_2) (fig. 3b, fig. 4b). Under cathodic biasing, electric charges are accumulated on both sides of the dielectric layer (fig. 6c), which increases locally the electric field. When the electric field reaches a sufficient value, breakdown occurs (fig. 6d). Cathodic breakdown causes local spalling of the layer (fig. 1). This provokes the electrical contact between the metal electrode and the electrolyte. Consequently, a large part of the charges flows through large porosities caused by spalling and thus limits charge accumulation (fig. 6e). However, in some places, charge accumulation can be sufficient to reach the breakdown electric field and therefore to lead to breakdown, but to a lesser extent than previously (fig. 6f). After 16 ± 2 cycles of accumulation/breakdown [16], charge accumulation is made impossible due to the increase in the number of shortcuts (fig. 6g) which quickly evacuate charges. Then, MDs eventually stop before the end of the cathodic period (fig. 1b in [16]).

Cathodic micro-discharges in alkaline-silicate electrolytes

NH_4F electrolytes offer adequate conditions to observe and study cathodic MDs. However, the aforementioned results show that those conditions are not fairly suitable for any industrial application due to poor layer properties. To grow thicker and denser layers on magnesium, alkaline-silicate electrolytes are often preferred [9, 22-24]. In these conditions, many anodic MDs are ignited and form an oxide layer at high rate. Unexpectedly, cathodic MDs can also appear in alkaline-silicate electrolyte (fig. 7). The cathodic MDs that appear in alkaline-silicate electrolyte show an oscillating pseudo-periodic behaviour as it was observed in NH_4F (inset fig. 7). However MDs appear during a shorter time (300-600 μs) in alkaline-silicate than in NH_4F electrolyte (1.7-2.1 ms) [16].

Figure 8 shows the evolution of light emission in the WAVE4 regime. Thanks to this regime, we remark that if a cathodic half-period follows an anodic half-period, then cathodic MDs can be observed. On the other hand, no MDs are observed during the cathodic half-period if it is not preceded by an anodic alternation. The presence of a prior anodic half-period is the condition for the appearance of cathodic MDs, irrespective of the electrolyte composition.

3.5 The influence of cathodic half-period on anodic MDs

In the WAVE5 regime, cathodic MDs are observed during the cathodic half-period when generated (fig. 9a). If a cathodic half-period is generated, the anodic overall light emission increases slightly (from 2 to 6 a.u.) during the next anodic half-period. On the other hand, if no prior cathodic half-period is generated, the anodic light emission is more intense at the beginning of the anodic half-period and then decreases by a factor of 2. The size of MDs follows a similar trend, increasing from 0.15 to 0.25 mm² after a cathodic half-period; and decreasing from 0.3 to 0.15 mm² without cathodic half-period (fig. 9c). Furthermore, the number of MDs is not affected by the presence of prior cathodic MDs (fig. 9d). The lifetime of anodic MDs increases very slightly (from 75 to 150 μ s) after a cathodic half-period, but it decreases otherwise from 200 to 100 μ s.

4. Conclusion

Layers grown in NH₄F are composed of MgO and MgF₂. Although MDs only appears during the cathodic half-period, these oxide layers grow during the anodic half-period. Moreover, an anodic half-period is necessary to observe MDs during the next cathodic half-period. However, NH₄F

electrolyte is not suitable in order to grow protective layers because of both corrosion of the substrate during anodic half-periods, and spalling of the layer by cathodic MDs.

On the other hand, cathodic half-period also influences the properties of anodic MDs. Without cathodic half-period, the formation of large and long MDs is promoted. These conditions are considered as responsible for higher defects concentration and roughness of the coatings [7]. Furthermore, cathodic half-period promotes shorter and smaller MDs, these conditions being favourable to get thicker and more homogeneous layers [6].

A correct setting of electric parameters is then essential to optimize coating quality. If cathodic MDs must be avoided, the presence of a cathodic half-period is mandatory to form layers with good properties.

5. Acknowledgment

We greatly acknowledge the Conseil Régional de Lorraine for granting A. Nominé's PhD work under decision 11CP-769.

6. References

- [1] A. L. Yerokhin, X. Nie, A. Leyland, A. Matthews, S. J. Dowey, « Plasma electrolysis for surface engineering », *Surf. Coat. Technol.* 122 (1999) 73-93
- [2] I. Shchedrina, A. G. Rakoch, G. Henrion, J. Martin, « Non-destructive methods to control the properties of MAO coatings on the surface of 2024 aluminium alloy », *Surf. Coat. Technol.* 238 (2014) 27-44
- [3] L. R. Krishna, A. S. Purnima, G. Sundararajan, « A comparative study of tribological behavior of microarc oxidation and hard-anodized coatings », *Wear* 261 (2006) 1095-1101
- [4] P. Bala Srinivasan, J. Liang, R. G. Balajee, C. Blawert, M. Störmer, W. Dietzel, « Effect of pulse frequency on the microstructure, phase composition and corrosion performance of

a phosphate-based plasma electrolytic oxidation coated AM50 magnesium alloy », *Appl. Surf. Sci.* 256 (2010) 3928-3935

- [5] J.-H. Wang, M.-H. Du, F.-Z. Han, J. Yang, « Effects of the ratio of anodic and cathodic currents on the characteristics of micro-arc oxidation ceramic coatings on Al alloys », *Appl. Surf. Sci.* 292 (2014) 658-664
- [6] J. Martin, A. Melhem, I. Shchedrina, T. Duchanoy, A. Nominé, G. Henrion, T. Czerwicz, T. Belmonte, « Effects of electrical parameters on plasma electrolytic oxidation of aluminium », *Surf. Coat. Technol.* 221 (2013) 70-76
- [7] A. Melhem, G. Henrion, T. Czerwicz, J. L. Briançon, T. Duchanoy, F. Brochard, T. Belmonte, « Changes induced by process parameters in oxide layers grown by the PEO process on Al alloys », *Surf. Coat. Technol.* 205 (2011) S133-S136
- [8] C. S. Dunleavy, J. A. Curran, T. W. Clyne, « Time dependent statistics of plasma discharge parameters during bulk AC plasma electrolytic oxidation of aluminium », *Appl. Surf. Sci.* 268 (2013) 397-409
- [9] R. Arrabal, E. Matykina, T. Hashimoto, P. Skeldon, G. E. Thompson, « Characterization of AC PEO coatings on magnesium alloys », *Surf. Coat. Technol.* 203 (2009) 2207-2220
- [10] E. Matykina, A. Berkani, P. Skeldon, G. E. Thompson, « Real-time imaging of coating growth during plasma electrolytic oxidation of titanium », *Electrochim. Acta* 53 (2007) 1987-1994
- [11] A. L. Yerokhin, L. O. Snizhko, N. L. Gurevina, A. Leyland, A. Pilkington, A. Matthews, « Discharge characterization in plasma electrolytic oxidation of aluminium », *J. Phys. Appl. Phys.* 36 (2003) 2110
- [12] S. Stojadinović, R. Vasilić, M. Petković, L. Zeković, « Plasma electrolytic oxidation of titanium in heteropolytungstate acids », *Surf. Coat. Technol.* 206 (2011) 575-581
- [13] S. Stojadinović, J. Jovović, M. Petković, R. Vasilić, N. Konjević, « Spectroscopic and real-time imaging investigation of tantalum plasma electrolytic oxidation (PEO) », *Surf. Coat. Technol.* 205 (2011) 5406-5413
- [14] F. Jaspard-Mécuson, T. Czerwicz, G. Henrion, T. Belmonte, L. Dujardin, A. Viola, J. Beauvir, « Tailored aluminium oxide layers by bipolar current adjustment in the Plasma Electrolytic Oxidation (PEO) process », *Surf. Coat. Technol.* 201 (2007) 8677-8682
- [15] F. Mécuson, T. Czerwicz, T. Belmonte, L. Dujardin, A. Viola, G. Henrion, « Diagnostics of an electrolytic microarc process for aluminium alloy oxidation », *Surf. Coat. Technol.* 200 (2005) 804-808
- [16] A. Nomine, J. Martin, C. Noel, G. Henrion, T. Belmonte, I. V. Bardin, V. L. Kovalev, A. G. Rakoch, « The evidence of cathodic micro-discharges during plasma electrolytic oxidation process », *Appl. Phys. Lett.* 104 (2014) 081603

- [17] S. Bardin, J.-L. Briançon, F. Brochard, V. Martin, Y. Zayachuk, R. Hugon, J. Bougdira, « Investigating Transport of Dust Particles in Plasmas », *Contrib. Plasma Phys.* 51 (2011) 246-251
- [18] N. Endstrasser, F. Brochard, V. Rohde, M. Balden, T. Lunt, S. Bardin, J.-L. Briançon, R. Neu, « Video tracking and post-mortem analysis of dust particles from all tungsten ASDEX Upgrade », *J. Nucl. Mater.* 415 (2011) S1085-S1088
- [19] P. Bruggeman, D. Schram, M. Á. González, R. Rego, M. G. Kong, C. Leys, « Characterization of a direct dc-excited discharge in water by optical emission spectroscopy », *Plasma Sources Sci. Technol* 18 (2009) 025017
- [20] P. Bruggeman, C. Leys, « Non-thermal plasmas in and in contact with liquids », *J. Phys. Appl. Phys.* 42 (2009) 053001
- [21] A. Hamdan, I. Marinov, A. Rousseau, T. Belmonte, « Time-resolved imaging of nanosecond-pulsed micro-discharges in heptane », *J. Phys. Appl. Phys.* 47 (2014) 055203,
- [22] H. Duan, C. Yan, F. Wang, « Growth process of plasma electrolytic oxidation films formed on magnesium alloy AZ91D in silicate solution », *Electrochim. Acta* 52 (2007) 5002-5009
- [23] H. Duan, C. Yan, F. Wang, « Effect of electrolyte additives on performance of plasma electrolytic oxidation films formed on magnesium alloy AZ91D », *Electrochim. Acta* 52 (2007) 3785-3793
- [24] J. Liang, P. B. Srinivasan, C. Blawert, M. Störmer, W. Dietzel, « Electrochemical corrosion behaviour of plasma electrolytic oxidation coatings on AM50 magnesium alloy formed in silicate and phosphate based electrolytes », *Electrochim. Acta* 54 (2009) 3842-3850

Table captions

Table 1 Composition of EV31 alloy.

Table 2 Current waveforms used in the present work.

Figure captions

Figure 1: Top-view secondary electron micrographs showing the surface of the layer grown in NH_4F electrolytes after a 40 min treatment in the bipolar DC pulse (WAVE1) regime.

Figure 2: Backscattered electron micrographs of cross sections of layers grown in NH_4F electrolytes during 40 minutes in the bipolar DC pulse (WAVE1) regime, at different magnifications.

Figure 3: EDX spectra (a) and XRD pattern (b) of a coating grown in NH_4F electrolytes after 40 minutes.

Figure 4: Chronogram of the current waveform and light emission in the negative DC pulse (WAVE2) regime.

Figure 5: Chronogram of current waveform and light emission (a) and backscattered electron micrographs (b) obtained after a 15-minute treatment in the positive DC pulse (WAVE3) regime.

Figure 6: Mechanism of cathodic breakdown.

Figure 7: Evolution of light emission (a), voltage (b) and current (c) in the bipolar regime in alkaline-silicate electrolyte. Note that time and current parameters are slightly different from those of WAVE1.

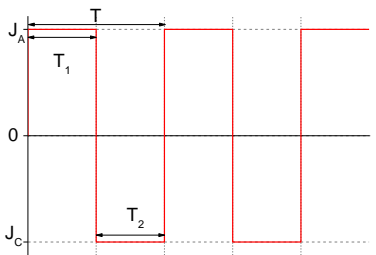
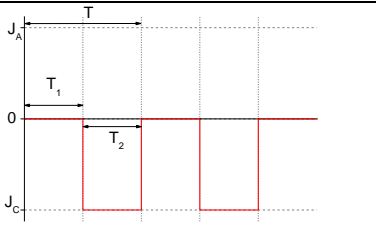
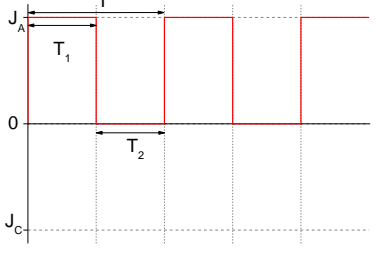
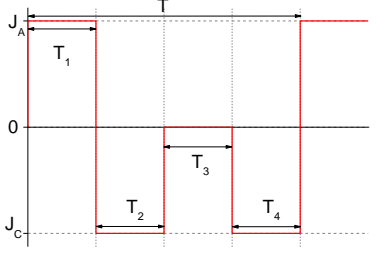
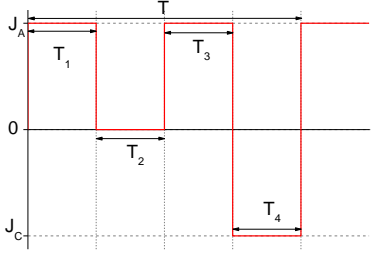
Figure 8: Evolution of light emission and current in the negative hybrid regime (WAVE4) in alkaline-silicate electrolyte.

Figure 9: Evolution of current (a) light emission (b) size (c) number (d) and lifetime (e) of micro-discharges under positive hybrid current (WAVE5) regime.

Table 1: Composition of EV31 alloy.

Element	Mg	Nd	Gd	Zn	Zr
wt %	Balance	2.86	1.38	0.25	0.66

Table 2: Current waveforms used in the present work.

Waveform	Schematic	J_A	J_C	T_1	T_2	T_3	T_4	T
		A/dm ²		ms				
WAVE1 (bipolar DC pulse)		20	-20	5	5	-	-	10
WAVE2 (negative DC pulse)		0	-8	5	5	-	-	10
WAVE3 (positive DC pulse)		8	0	5	5	-	-	10
WAVE4 (negative hybrid)		12	-20	6	4	6	4	20
WAVE5 (positive hybrid)		20	-12	4	6	4	6	20

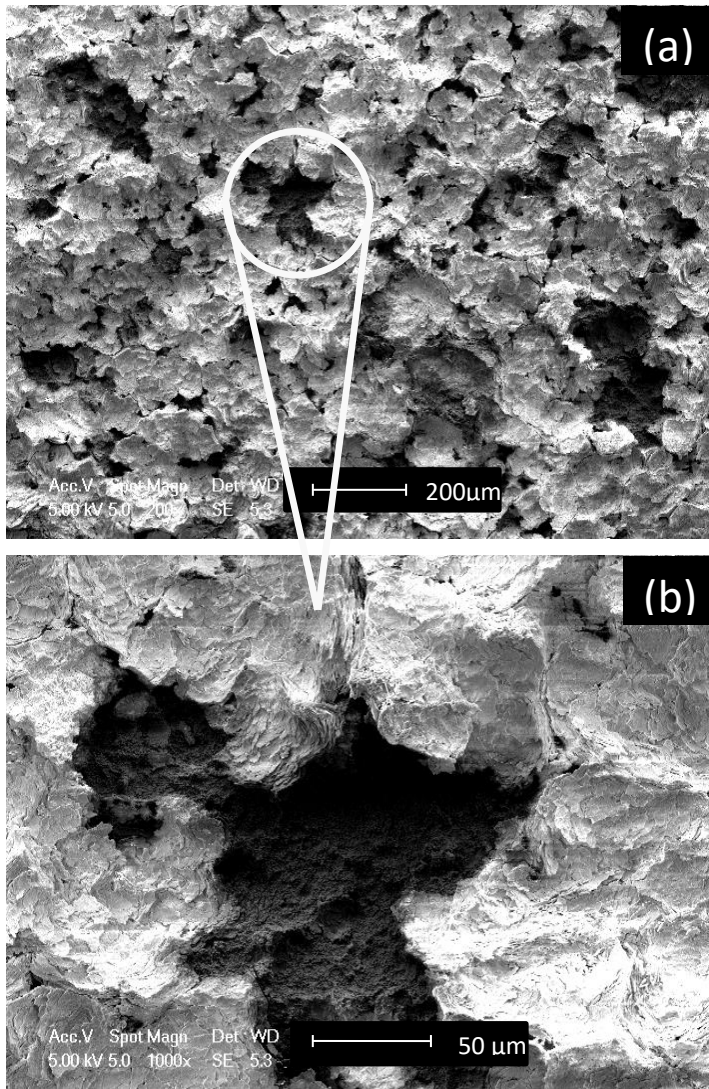


Figure 1: Top-view secondary electron micrographs showing the surface of the layer grown in NH_4F electrolytes after a 40 min treatment in the bipolar DC pulse (WAVE1) regime.

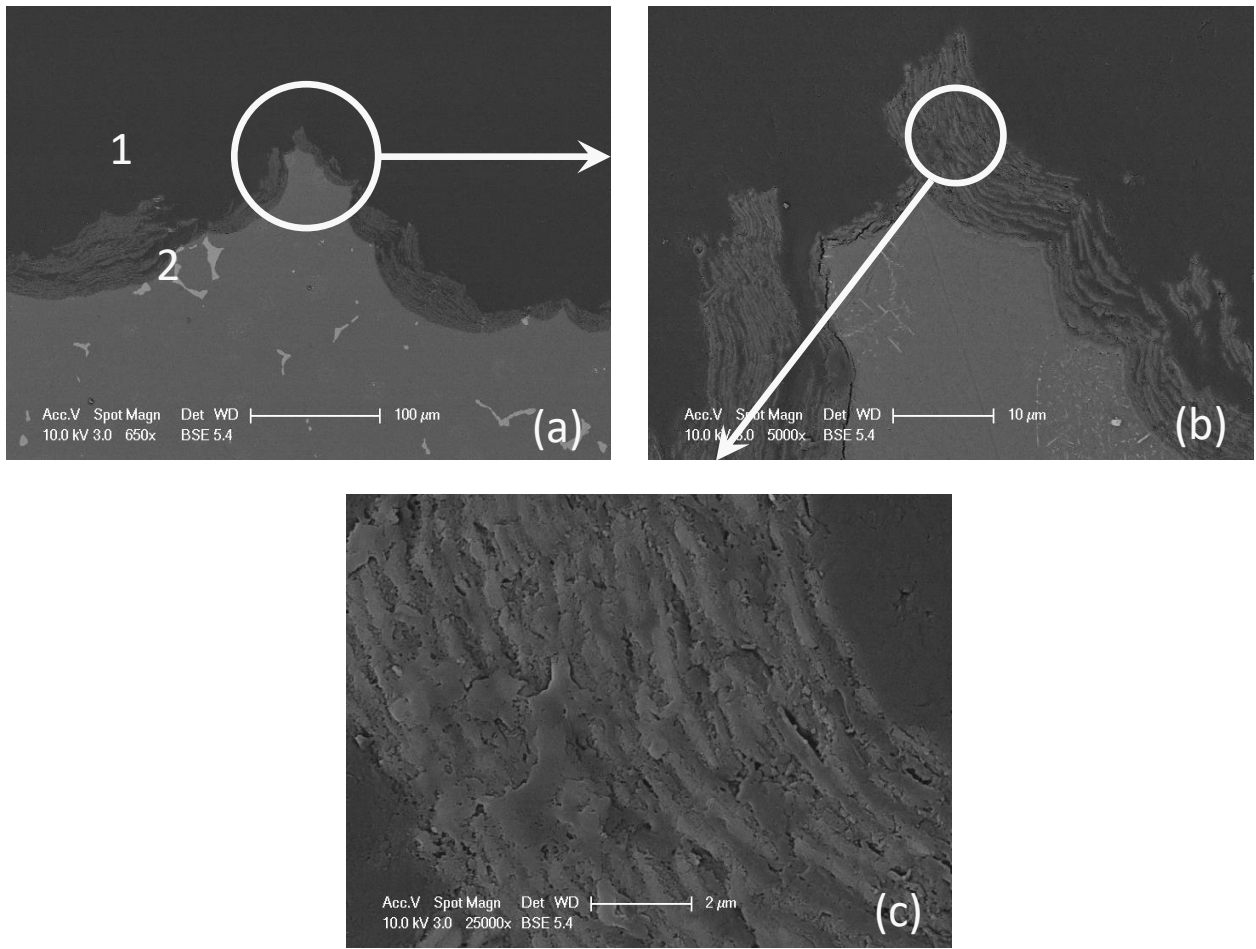


Figure 2: Backscattered electron micrographs of cross sections of layers grown in NH_4F electrolytes during 40 minutes in the bipolar DC pulse (WAVE1) regime, at different magnifications.

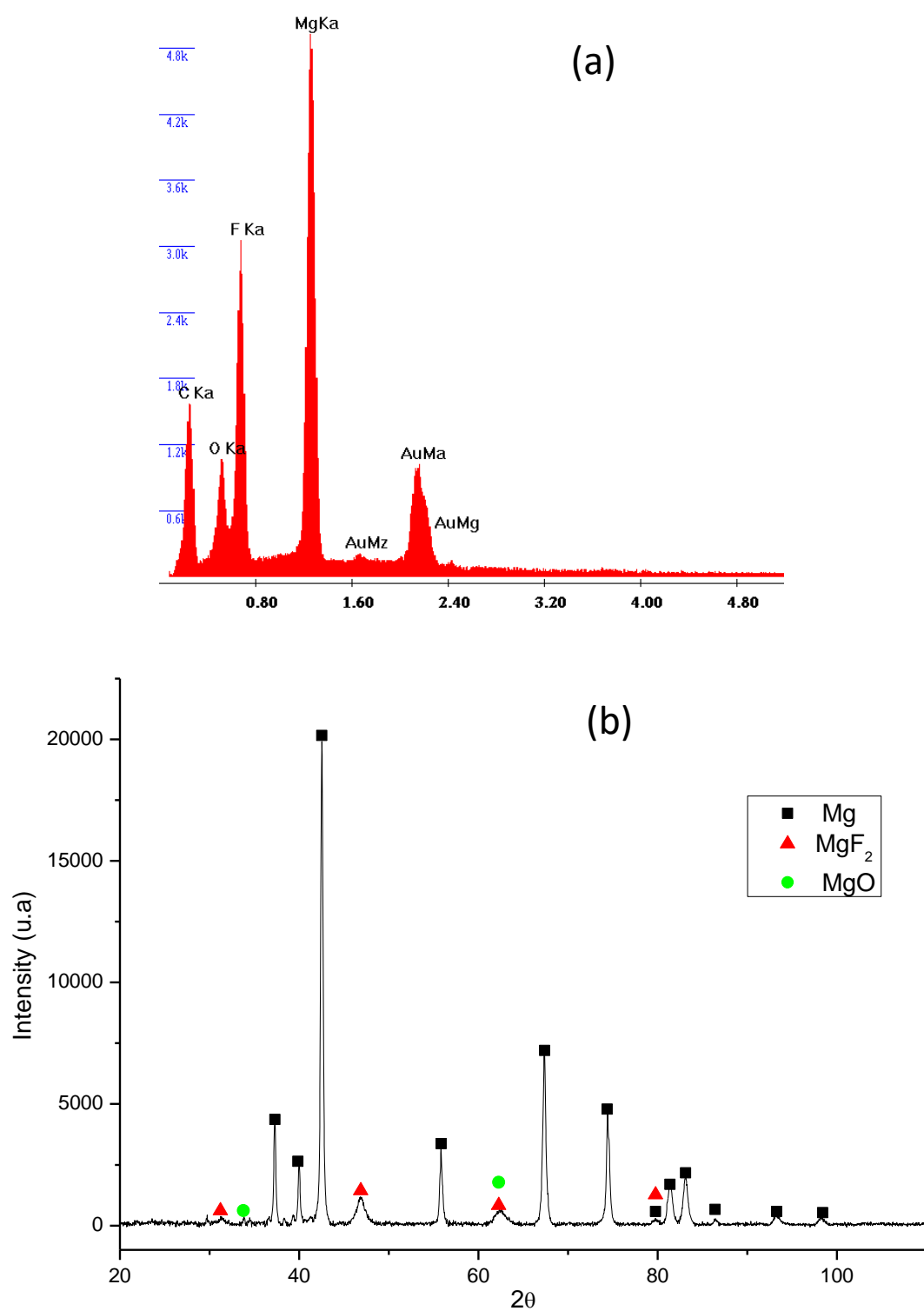


Figure 3: EDX spectra (a) and XRD pattern (b) of a coating grown in NH_4F electrolytes after 40 minutes.

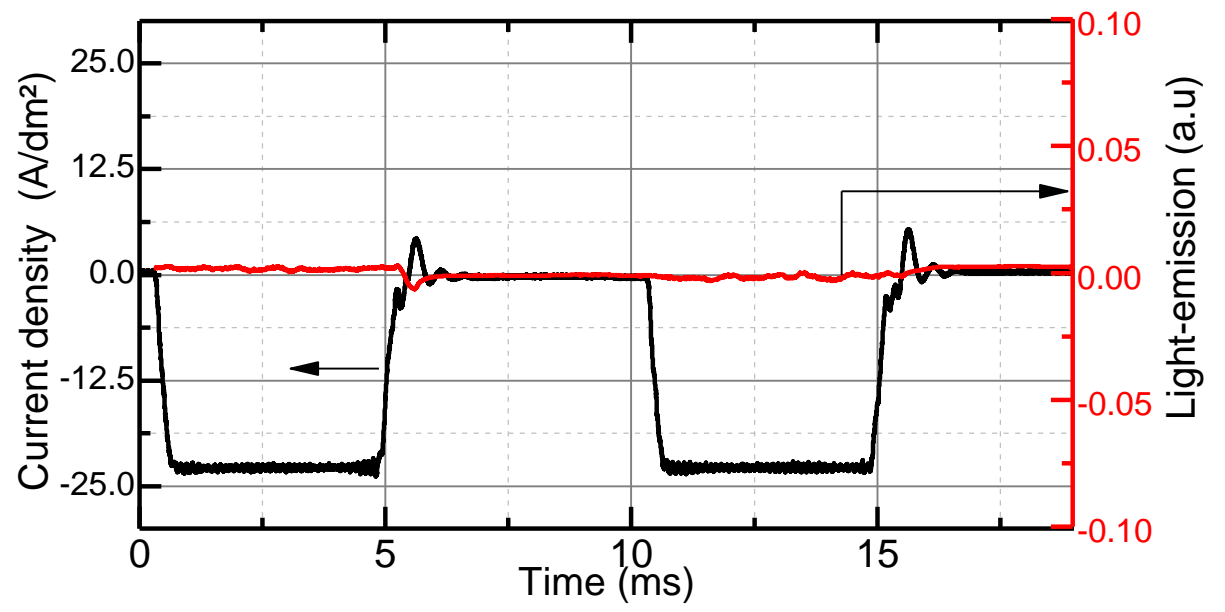


Figure 4: Chronogram of the current waveform and light emission in the negative DC pulse (WAVE2) regime.

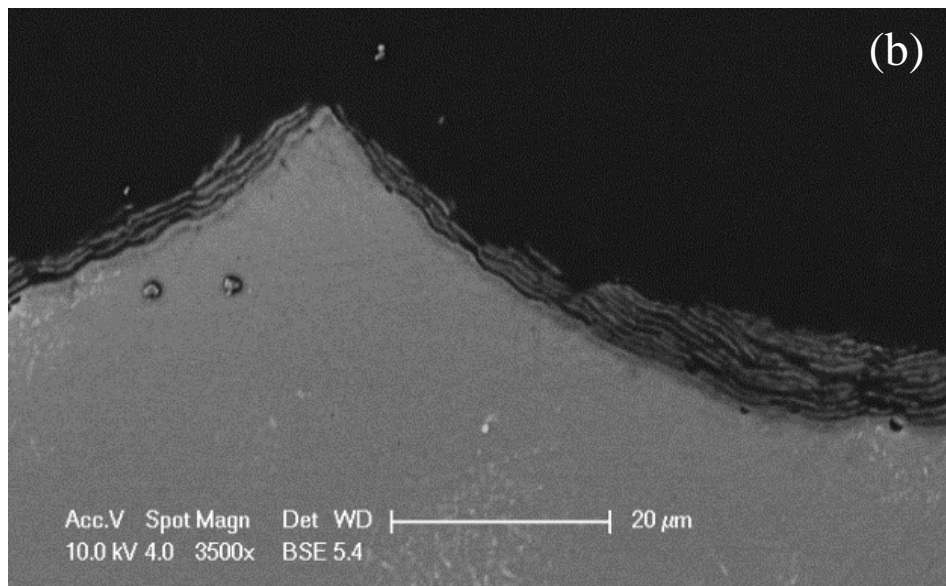
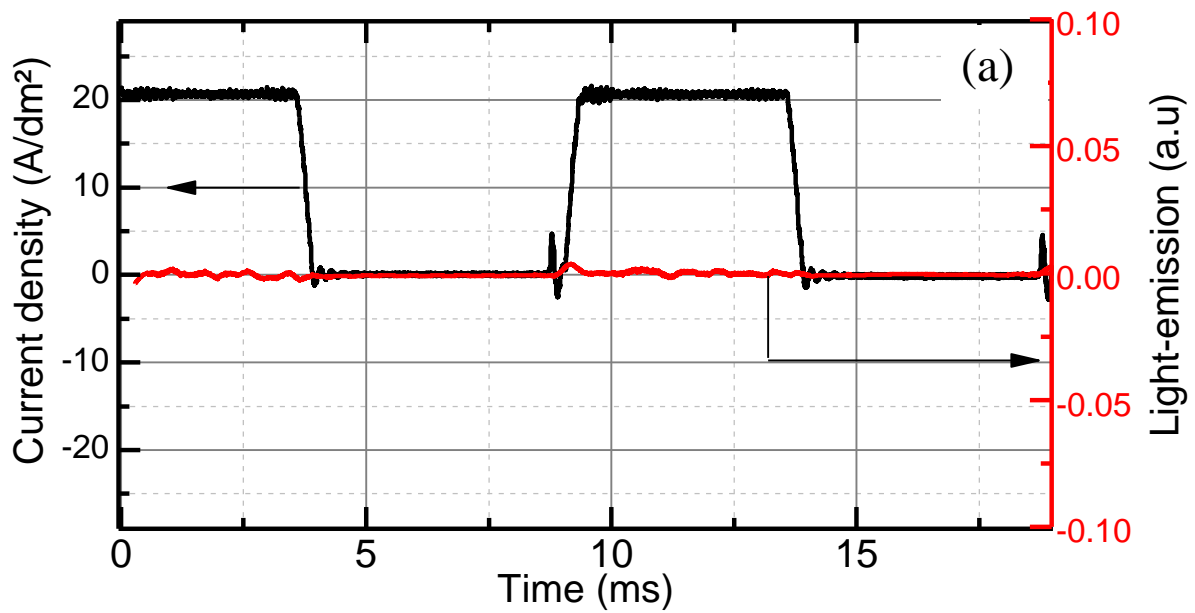


Figure 5: Chronogram of current waveform and light emission (a) and backscattered electron micrographs (b) obtained after a 15-minute treatment in the positive DC pulse (WAVE3) regime.

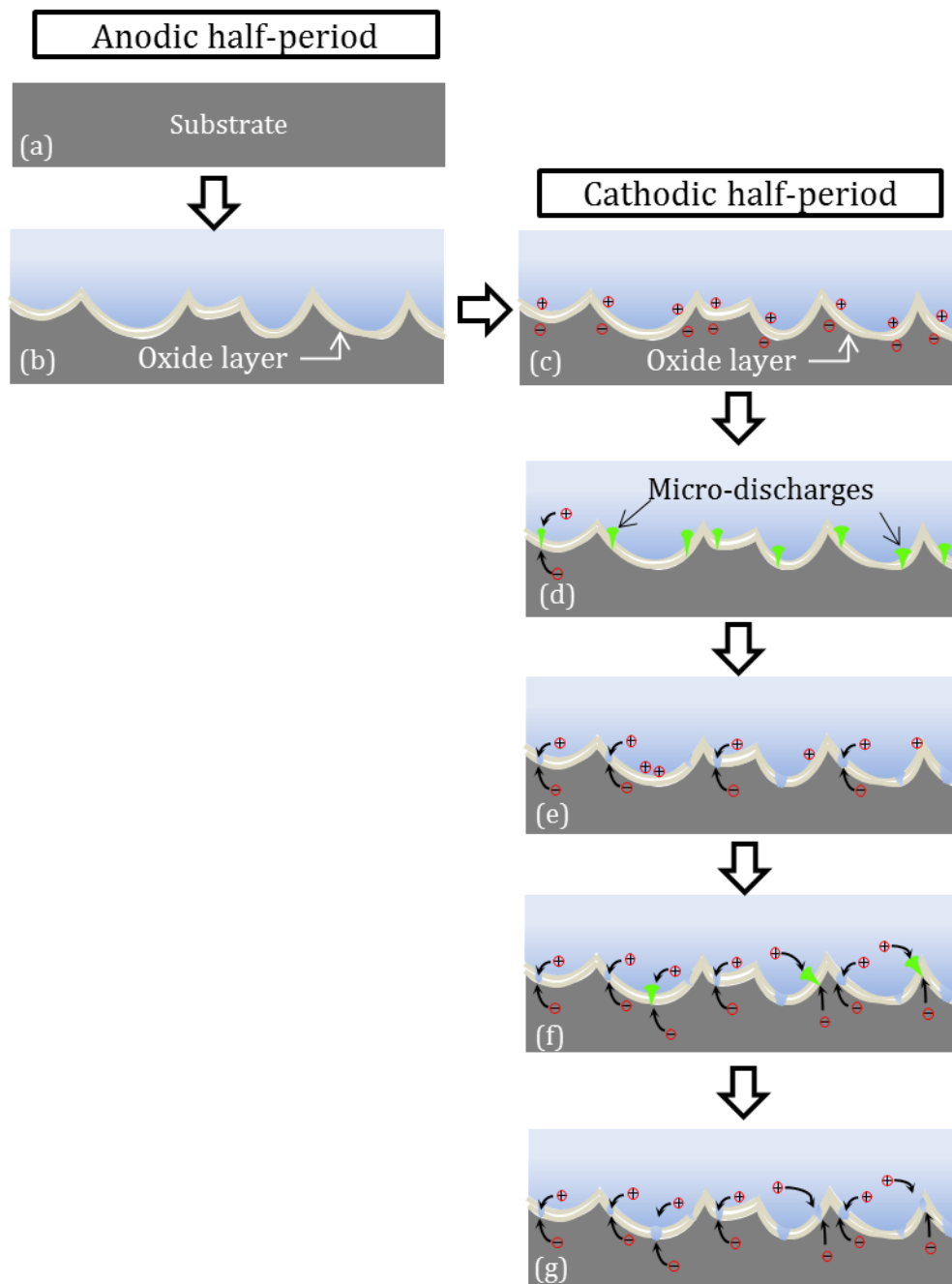


Figure 6: Mechanism of cathodic breakdown.

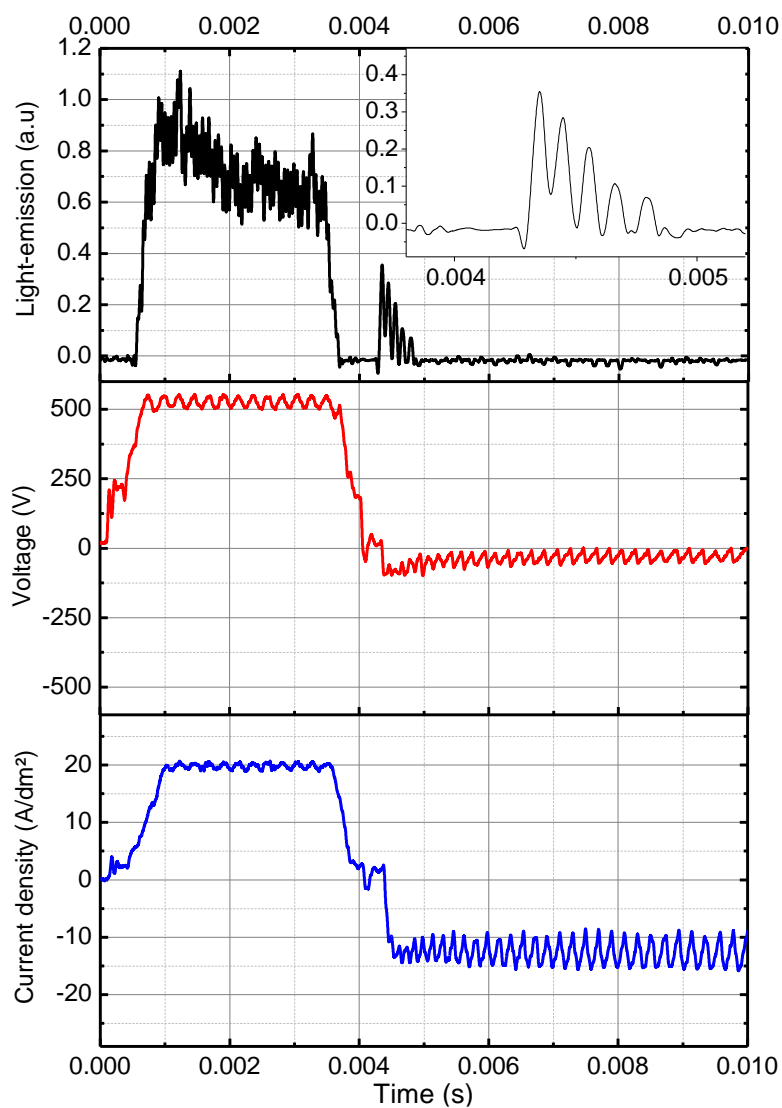


Figure 7: Evolution of light emission (a), voltage (b) and current (c) in the bipolar regime in alkaline-silicate electrolyte. Note that time and current parameters are slightly different from those of WAVE1.

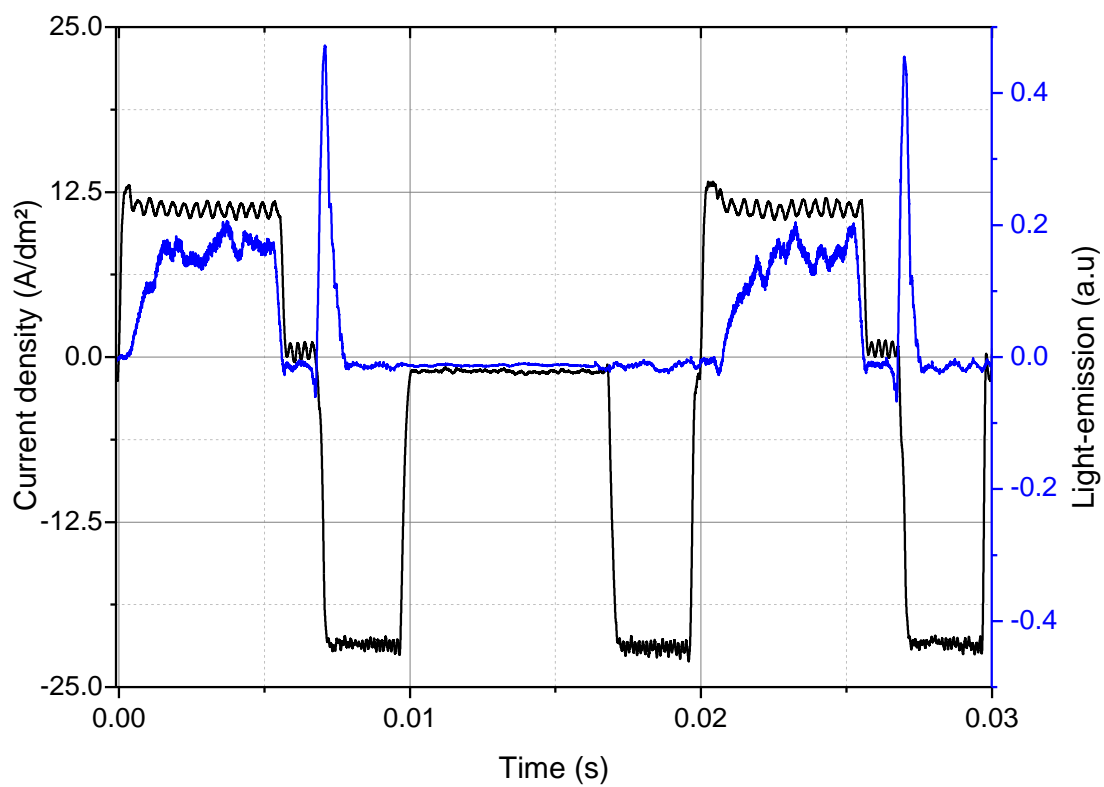


Figure 8: Evolution of light emission and current in the negative hybrid regime (WAVE4) in alkaline-silicate electrolyte.

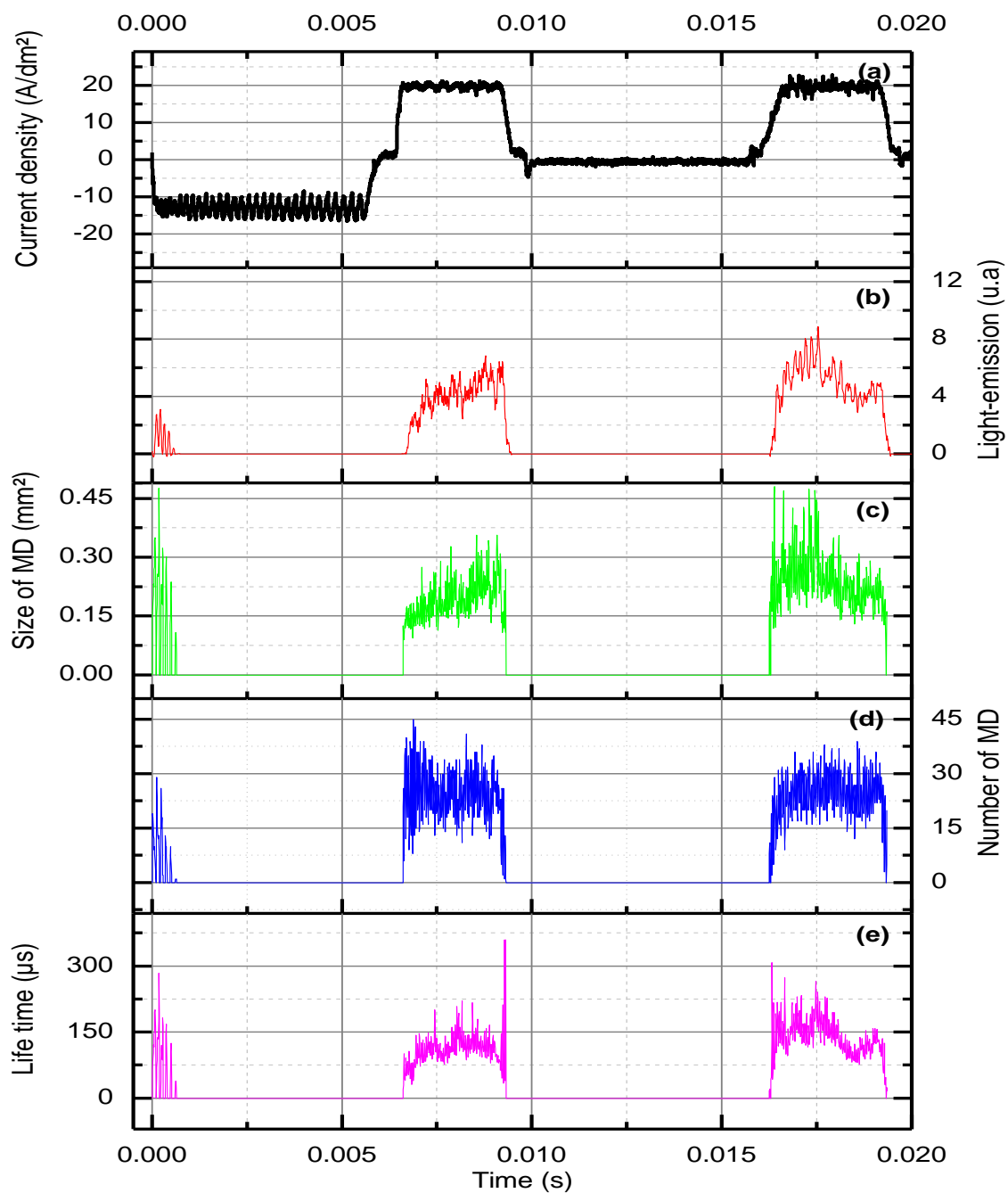


Figure 9: Evolution of current (a) light emission (b) size (c) number (d) and lifetime (e) of micro-discharges under positive hybrid current (WAVE5) regime.